Materials Today Communications 34 (2023) 105440

Contents lists available at ScienceDirect

Materials Today Communications

journal homepage: www.elsevier.com/locate/mtcomm

Copper coatings on poly(lactic acid) via rapid magnetron sputtering: Morphology, chemistry, and antimicrobial performance against bacteria and SARS-CoV-2

Daniel J. da Silva [a], Greiciele S. Ferreira [a], Adriana Duran [a], Fernando L.A. Fonseca [b], Duclerc F. Parra [c], Rodrigo F. Bueno [a,d], Derval S. Rosa [a,*]

[a] Center for Engineering, Modeling, and Applied Social Sciences (CECS), Federal University of ABC (UFABC), Av. dos Estados, 5001, Bangú, Santo André, SP, Brazil
[b] Faculty of Medicine of ABC (FMABC), Department of Clinical Analysis, Av. Lauro Gomes, 2000, Santo André, SP, Brazil
[c] Nuclear and Energy Research Institute, IPEN-CNEN/SP, Av. Prof. Lineu Prestes, 2242 São Paulo, SP, Brazil
[d] Coordinator of the COVID-19 Monitoring Network in Wastewater National Water and Basic Sanitation Agency, Ministry of Science, Technology and Innovation and Ministry of Health, Brazil

ARTICLE INFO

Keywords:
SARS-CoV-2
PLA
Copper
Plasma
Coating
Antimicrobial

ABSTRACT

Materials with antimicrobial properties are highly desirable for making food packaging and personal protective equipment due to their intrinsic ability to prevent the proliferation of pathogenic microorganisms and food contamination. Poly(lactic acid) (PLA) is a biodegradable, compostable, and recyclable polymer that presents interesting mechanical properties for such applications. However, this polymer does not show intrinsic antimicrobial activity. Herein, we applied Radio Frequency Magnetron Sputtering (RF-MS) to produce antimicrobial copper coatings on the PLA surface. The results indicate that the prolongation in the copper deposition time causes an increase in surface roughness. The PLA coating with copper using a short deposition time (5–20 s) was sufficient to guarantee a bactericidal effect against *Escherichia coli* and *Bacillus subtilis*, in addition to conferring antiviral activity against Omicron Severe Acute Respiratory Syndrome Coronavirus 2 (SARS-CoV-2). Nuclear magnetic resonance (NMR) and high-resolution x-ray photoelectron (XPS) spectroscopic studies indicate that occurs only localized degradation on the PLA surface via polymer chain scission. The RF-MS technique was suitable for rapidly manufacturing antimicrobial Cu-coated PLA and providing low copper consumption in the antimicrobial coating process.

1. Introduction

Microbial adhesion and its proliferation on solid surfaces can form a biofilm with particular physicochemical and biochemical features that can cause the failure of devices used in engineering, dentistry, medicine, and other critical technological applications [1–4]. Materials with antibacterial properties are also highly desirable for making food packaging and personal protective equipment (PPE) because they can prevent the proliferation and transmission of pathogenic microorganisms that can compromise human health.

Among the material available currently, poly(lactic acid) (PLA) stands out due to being a thermoplastic polyester with biocompatible and biodegradable characteristics, which can be recycled and synthesized by step-growth polymerization of lactic acid, involving solvents and high vacuum [5]. This synthetic route mainly leads to low molar mass PLA due to water and impurities in the reaction medium. Another synthetic route is the ting-opening polymerization of lactide without using solvents. This technique makes it possible to obtain PLA with a higher molar mass than the polycondensation of lactic acid [5]. Due to the presence of chiral carbon, lactic acid, and lactide present optical isomers, lactic acid can form two optical isomers: L-lactic acid and D-lactic acid. In addition to the L and D stereoisomers, lactide has a meso isomer. Lactic acid obtained by the fermentation of carbohydrates is predominantly levorotatory. The petrochemical route obtains a 50/50 racemic mixture of lactic acid enantiomers. For this reason, there are several distinct forms of PLA depending on the monomeric units used [6]: poly(L-lactic acid) (PLLA) which is synthesized with levorotatory monomers; poly(D-lactic acid) (PDLA) which is synthesized with

* Corresponding author.
E-mail address: dervalrosa@yahoo.com.br (D.S. Rosa).

https://doi.org/10.1016/j.mtcomm.2023.105440
Received 16 October 2022; Received in revised form 10 January 2023; Accepted 16 January 2023
Available online 18 January 2023

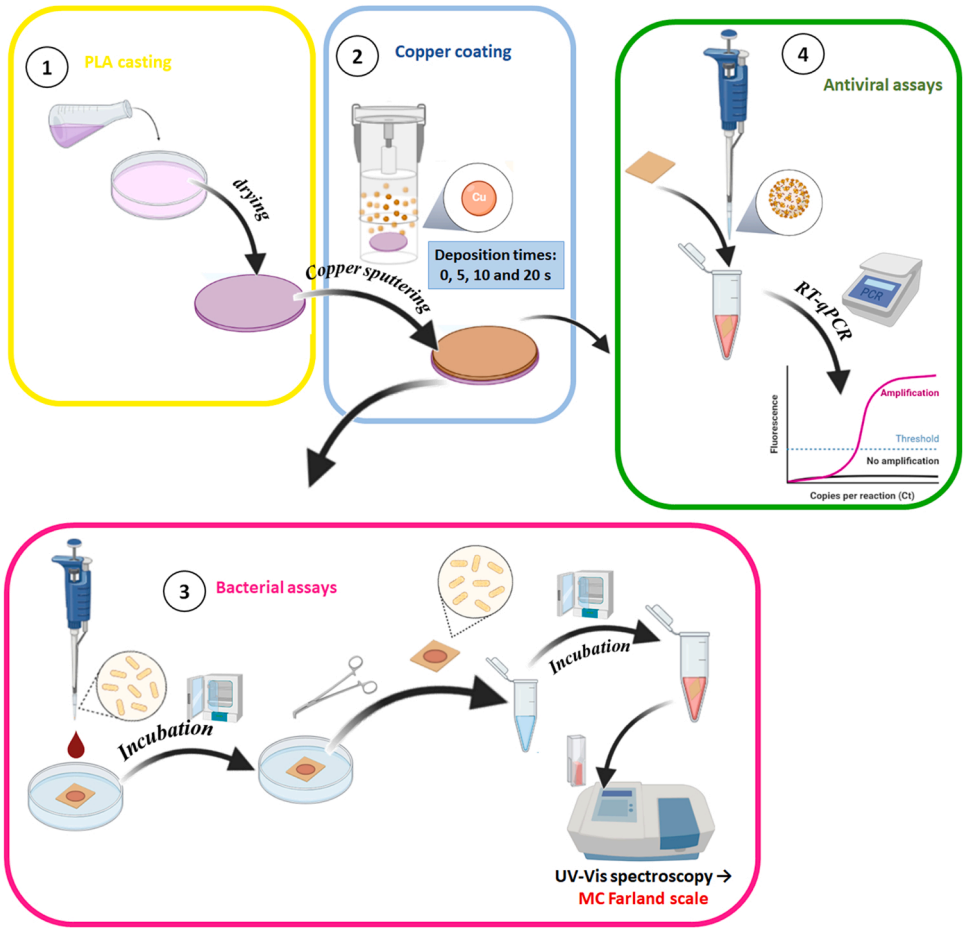

Fig. 1. Illustrative representation of the PLA casting, copper coating procedure of the PLA films by radio frequency magnetron sputtering (RF-MS), and antimicrobial assays.

dextrorotatory monomers; and poly(DL-lactic acid) (PDLLA) which is obtained by polymerizing a racemic mixture of monomers.

Besides the petrochemical route, lactic acid (PLA monomer) can be produced from renewable biomass, including bacterial fermentation of sugar or starch from vegetables. In recent years, bacterial fermentation has been the most used option as it is a more eco-friendly route [7]. This possibility of PLA being synthesized from natural sources, combined with its recyclability, has attracted interest in the use of this polymer as an alternative polymeric material to mitigate the environmental impacts caused by unsustainable synthetic polymers widely used in several sectors, such as polypropylene (PP), polyethylenes (PEs), polystyrene (PS) and other petroleum-based polymers [8].

Traditionally, the technological methods for preventing the development of biofilms are based on chemical modification of the material surface by chemical functionalization or by adding biocidal substances. These strategies aim to prevent microbial attachment (anti-biofouling property) or kill microorganisms (antifungal, antiviral, bactericidal, or biocidal properties) when it comes into direct contact with the solid surface by biochemical mechanisms [9]. Generally, bactericidal and anti-fouling properties are introduced into PLA by adding antimicrobial agents to the polymer bulk or surface chemical modification [10–13].

The use of metals or metallic nanoparticles to make antimicrobial polymeric products has attractive potential applications, particularly in biomedical applications, food packaging and PPE, due to their virucidal and bactericidal properties [14,15]. Silver, gold, platinum, and copper are the major metals with intrinsic viricidal properties used for these industrial applications [16,17]. In addition to these materials, metal oxides with virucidal action are used for the same purpose, including ZnO, SiO_2, TiO_2, and CuO [17–19].

The sanitizing properties of copper have long been known against bacteria, viruses, and fungi. Like silver, copper (Cu) has antimicrobial activity through oxidative stress and the release of metal ions that cause irreversible damage to structural molecules in the biological systems (proteins, lipids, and nucleic acids). An advantage of copper is that bacterial copper resistance systems do not provide protection against bacterial cell death by direct contact but only prolong cell survival [20,21]. Moreover, the lowest cost of copper is another advantage of this metal concerning using silver as a self-disinfecting agent. For this reason, copper is more attractive than silver from an economic point of view. Furthermore, forming a passivating layer of copper oxides does not compromise their antimicrobial activity, as they also have intrinsic self-disinfecting properties associated with generating reactive oxygen species (ROS) [22,23]. From an environmental point of view, copper metal and copper oxides are mildly toxic [17,24].

The surface modification of polymers by low-temperature plasmas (or cold plasmas, non-thermal plasmas) is a feasible process for polymer surface modifications involving chemical and physical processes, which has been used by the industry [25]. The physical processes are associated with the bombardment of the polymeric surface by ions and electrons present in the plasma, causing mainly changes in the roughness surface due to the removal/ablation of material on the surface. In another way, the chemical processes correspond to chemical reactions between plasma particles with molecules on the polymer surface, which cause breakage and formation of chemical bonds, often leading to changes in chemical functional groups on the polymer surface [26].

Among the low-temperature plasma technologies, the magnetron

sputtering technique is suitable for generating plasma with high density under lower pressure than conventional sputtering technologies (such as DC and RF diode bias sputtering), enabling a high ionization rate of secondary electrons to quickly metal deposition on substrates [27,28]. In this way, the substrate undergoes low damage due to its exposure to plasma, being very important in the surface treatment of polymers so that these materials are not substantially damaged and their macroscopic properties are undesirably modified.

Within this context, plasma treatment has been a convenient approach for binding functional groups and tuning the topography of polymer, enabling the design of PLA-engineered products for advanced applications [7,29–34]. However, there is a lack of studies about the bactericidal and antiviral activity of copper coating on PLA obtained by magnetron sputtering.

Given the scientific relevance, the antiviral performance of the Cu-coated PLA against the Omicron SARS-CoV-2 virus is reported in this work. This virus strain is a highly contagious variant of the coronavirus responsible for the pandemic of Coronavirus Disease 2019 (COVID-19), and there are no studies about the antiviral performance of Cu-coated PLA systems against Omicron SARS-CoV-2 virus [35]. The antiviral results from quantitative reverse transcription-polymerase chain reaction (RT-qPCR) indicate that the SARS-CoV-2 virions undergo damage to the genetic material. Also, the copper coating prevented the formation of *E. coli* and *B. subtilis* biofilms on the PLA surface. The copper coating approach reported here proved a viable technological alternative for producing antimicrobial copper coating for manufacturing biomedical devices and PPE with antimicrobial and anti-biofouling properties.

2. Experimental section

2.1. Materials

Chloroform ($CHCl_3$), ethylene glycol, and diiodomethane were supplied from Synth (São Paulo, Brazil) and used without further purification. Poly(lactic acid) (PLA) with a melt flow index of 9.1 ± 1.8 g/10 min (ASTM D-1238/13, 190 °C - 2.16 kg) was purchased from GTMAX3D - Equipamentos Eletrônicos e Materiais Plásticos LTDA (São Paulo, Brazil). Deuterated chloroform ($CDCl_3$) was purchased from Sigma Aldrich (São Paulo, Brazil).

2.2. PLA film preparation

PLA films with a thickness of 290 ± 80 μm were obtained by dissolving PLA in chloroform (2 $g.mL^{-1}$) at room temperature, introduced in glass dishes, and dried in semi-open desiccators under atmospheric pressure at 25 °C.

2.3. Copper coating by radio frequency magnetron sputtering (RF-MS)

The PLA films were coated in disc format (diameter = 70 mm). Then, they were put in an RF-MS reactor at 100 mm of distance from the target (Cu, 99.99% purity). The coating was performed under operating pressure of 100 Bar (Argon, 99.99%), using a Cu target (99.99% purity), a constant electric current (0.2 A), and a constant discharge power (40 W). Different copper deposition times were utilized in the experiments: 5, 10, and 20 s. Fig. 1 presents a schematic illustration of the coating method of the PLA films.

2.4. Characterizations

2.4.1. Atomic Force Microscopy (AFM)

The AFM images (area = 1 μm x 1 μm) of the PLA surfaces were obtained in a Multimode 8 microscope (Bruker, USA), using a silicon nitride probe (ScanAsyst-Air-HR type) with a characteristic spring constant of 0.4 $N.m^{-1}$ and a nominal resonant frequency of 130 kHz. The AFM analyses were performed with the peak force mode scanning, ScanAsyst method, scanning frequency of 3.5 Hz, and pixel resolution of 512 × 512.

Table 1
Surface tension data of the test liquids at 25 °C [41–44]: dispersive (γ_s^{LW}), acid (γ_s^+) and base (γ_s^-) of the liquid surface tension (γ_l^{total}).

Liquid	γ_l^{LW} (mJ m^{-2})	γ_l^p (mJ m^{-2})	γ_l^+ (mJ m^{-2})	γ_l^- (mJ m^{-2})	γ_l^{total} (mJ m^{-2})
Diiodometane	50.8	0	0	0	50.8
Water	21.8	51.0	25.5	25.5	72.8
Ethylene glycol	29.0	19.0	3.0	30.1	48.0

2.4.2. X-ray photoelectron spectroscopy (XPS)

XPS spectra were collected at room temperature using K-alpha equipment (Thermo Scientific, USA). The monochromatic radiation A1 Kα was used to collect all XPS high-resolution spectra at 10 eV acquired at 0.1 eV step interval and acquisition time of 0.5 s, using standard charge neutralization. XPS spectra were calibrated to give C-C binding energy (C1s region) of 284.63 eV. All XPS data analyses and curve fitting were performed in CasaXPS software (version 2.3.25), using U2 Tougaard background approximation and finite Lorentzian asymmetric (LF) lineshape (with relative sensitivity factors = 1). All XPS spectra were calibrated to give C-C/C-H binding energy (C1s region) of 284.8 eV, according to the literature data [36].

2.4.3. Contact angle and surface free energy (γ_s^{total}) measurements

The static contact angles (θ_{est}) were determined by a static/dynamic contact angle tensiometer (SEO model - Phoenix 300, Kromtech Alliance Corp., London, UK), using the sessile drop method with different test liquids: diiodomethane, water, and ethylene glycol. The measurements were performed under air relative humidity of 67 ± 5% and a temperature of 25 ± 2 °C, using 10 μL of the test liquid that was dropped on the surface's sample. The total surface free energy (γ_s^{total}) was calculated with the θ_{est}, according to the Young-Laplace equation and Lifshitz-van der Waals acid-base model (Eqs. 1 and 2). For this purpose, the θ_{est} values were previously converted to the corrected contact angles (θ_c), considering the Wenzel roughness factor (r) and the Cassie-Baxter factor (f) determined from AFM topographical data (Eq. 3), as detailed in the literature [37–39]. The surface tension data of the test liquids used in the calculations are detailed in Table 1.

$$\gamma_s^{total} = \gamma_s^{LW} + 2\sqrt{\gamma_s^+ \gamma_s^-} \tag{1}$$

$$\gamma_s^{LW} = \frac{\gamma_l^{LW}}{4}\left[1 + \cos(\theta_c^{apolar})\right]^2 \tag{2}$$

$$\cos(\theta_c) = \frac{\left[\cos(\theta_{est} + 1 - f\right]}{rf} \tag{3}$$

where γ_s^{LW}, γ_s^+ and γ_s^- are the dispersive, acid, and base components of γ_s^{total}, in that order. $\theta_c^{apolar}$is the contact angle measured with a standard non-polar liquid (diiodomethane, $\gamma_s^{LW} = 0$). γ_s^+ and γ_s^- are calculated from the θ_c data, using Eq. (4) [40].

$$\begin{bmatrix} \sqrt{\gamma_s^+} \\ \sqrt{\gamma_s^-} \end{bmatrix} = \frac{1}{2}\begin{bmatrix} \sqrt{\gamma_{l,1}^-} & \sqrt{\gamma_{l,1}^+} \\ \sqrt{\gamma_{l,2}^-} & \sqrt{\gamma_{l,2}^+} \end{bmatrix}^{-1} \begin{bmatrix} \gamma_{l,1}^p(1 + \cos(\theta_{c1}) - 2\sqrt{\gamma_{l,1}^{LW}\gamma_s^{LW}} \\ \gamma_{l,2}^p(1 + \cos(\theta_{c2}) - 2\sqrt{\gamma_{l,2}^{LW}\gamma_s^{LW}} \end{bmatrix} \tag{4}$$

where γ_l^{LW}, γ_l^+, γ_l^-, and γ_l^p are the surface tension parameters characteristic of two different polar test liquids (water and ethylene glycol), which are indicated by 1 and 2 indexes.

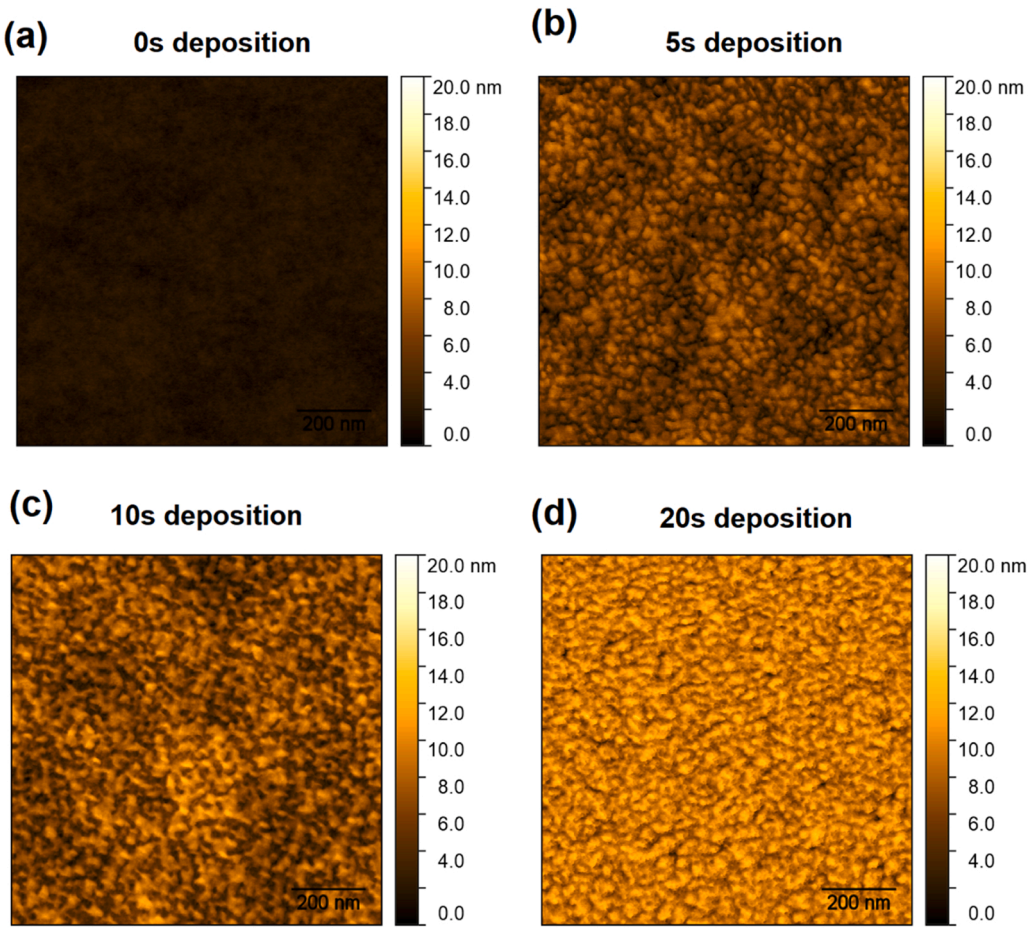

Fig. 2. AFM images of the PLA samples after different copper deposition times: (a) 0 s, (b) 5 s, (c) 10, and (d) 20 s. Scan area = 1 μm x 1 μm. Bar scales = 200 nm.

2.5. Nuclear magnetic resonance (NMR) spectroscopy experiments

All NMR spectra were recorded at 300 K on a 500 MHz infinity shield Varian spectrometer (Agilent, CA, USA). ^{1}H NMR spectra were acquired with a number of scans of 32, relaxation delay of 1 s, pulse angle of 45°, acquisition time of 6.4 s, spectral width of 5000 Hz, receiver gain of 46 dB, and 32,000 complex points. ^{13}C NMR spectra were acquired with a number of scans of 256, relaxation delay of 1 s, pulse angle of 45°, acquisition time of 1.152 s, spectral width of 27,777.8 Hz, receiver gain of 30 dB, and 32,000 complex points. ^{1}H-^{13}C HSQC bidimensional NMR experiments were performed with the number of scans per increment of 4, acquisition time of 0.150 s, spectral width of 5000 and 28,901.7 Hz for the proton and carbon, average $^{1}J_{C-H}$ of 146 Hz, receiver gain of 46 dB, coupling constant of 146 Hz, and 5000 complex points. Tetramethylsilane (TMS) was applied as an internal reference compound for NMR measurements. All PLA samples were dissolved in $CDCl_3$, and the copper coating did not affect the polymer solubility due to the low amount of metal on the surface of the Cu-coated PLA samples.

2.6. Antibacterial assays

The bactericidal assays were performed using a bacterial growth inhibition test in nutrient broth. The PLA samples (squares of 0.5 cm × 0.5 cm) were coated with 5 μL of *Escherichia coli* (*E. coli*, ATCC 25922) and *Bacillus subtilis* (*B. subtilis*, Caron Beta A 155) inoculums at a count of 10^5 CFU.mL^{-1}. Subsequently, the samples were incubated at 36 °C and 32 °C for *E. coli* and *B. subtilis* for bacterial growth for 24 h. then, they were added to a test tube containing 2 mL of nutrient culture medium (Kasvi nutrient broth) and incubated again for 72 h (*E. coli*) and 120 h (*B subtilis*). After incubation, a UV-Vis spectrophotometer (UV-M51 BEL, Bel Engineering srl) was used to quantify microorganisms using a wavelength absorption at 630 nm and MC Farland microbiology scale.

2.7. Antiviral assays

SARS-CoV-2 inoculation and detection of SARS-CoV-2 genetic material were performed as described previously [45]. The PLA samples (discs with diameter = 0.5 mm) were maintained in direct contact with Omicron SARS-CoV-2 inoculums (50 μL) for 30 min. The viral inoculums were collected with oropharynx and nasopharynx swabs from anonymous patients diagnosed with COVID-19, contaminated with the Omicron SARS-CoV-2 variant. RNA extraction process from frozen SARS-CoV-2 inoculums was performed with a commercial kit (PureLink™ Viral RNA Mini Kit - Invitrogen™). After the direct contact time, the SARS-CoV-2 genetic material was amplified by Quantitative reverse transcription-polymerase chain reaction (RT-qPCR) using the 2019-nCoV TaqMan RT-PCR kit (Norgen, Cat. TM67120), using CFX Opus Real-Time PCR Systems (Bio-Rad, USA) and three programmed reaction cycles (cycle 1 – 50 °C for 30 min; cycle 2 – 95 °C for 3 min; cycle 3–45 × 95 °C for 3 s; cycle 4–55 °C for 30 s). A negative control corresponds to water, and the positive control corresponds to the virus inoculum without direct contact with the PLA samples. N2 gene was the selected target on the RNA viral and used to make a standard calibration curve ($y = 3.723\ x + 44.75$; $R^2 = 0.998$; Efficiency = 85.6%, limit of detection (LOD) = 10 copies of the genome). The cycle threshold values (Ct values) from the RT-qPCR measurements were 39.77 ± 0.58.

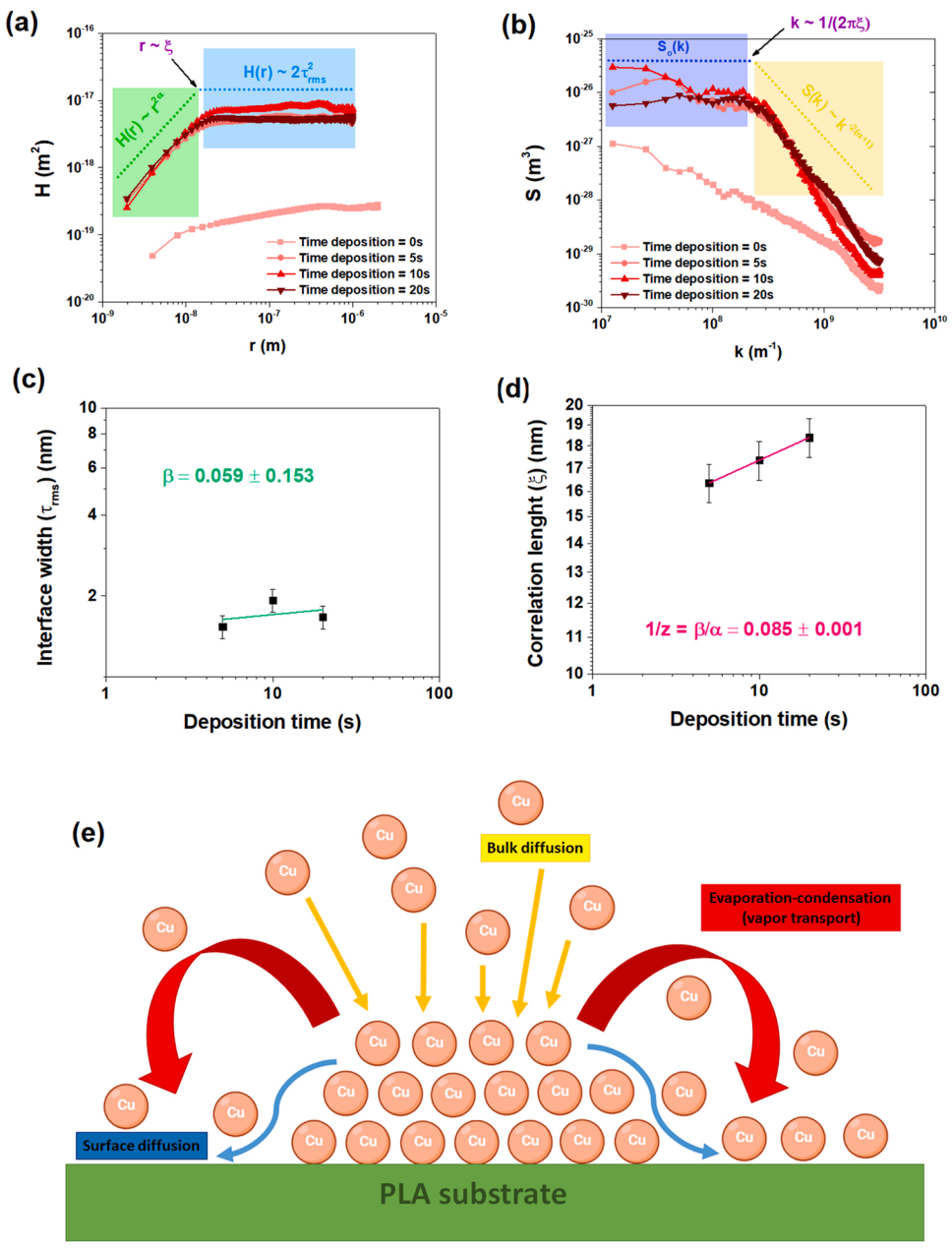

Fig. 3. Log-log plots for the (a) height-height correlation function H(r) versus length scale (r), (b) power spectral density function S(k) versus wave number (k), (c) root-mean-square (RMS) roughness (interface width, τ_{rms}) versus deposition time, and (d) lateral correlation length (ξ) versus deposition time for the PLA samples after different metal deposition times (0, 5, 10, and 20 s). (e) Illustration (out of scale) for the growth mechanisms of the copper thin film coating (evaporation-condensation of copper atoms due to local heating, bulk diffusion of copper atoms from the copper target to the PLA surface, and surface diffusion due to lateral copper atom transport occasioned by high atomic mobility enhanced by surface heating of the substrate). PSD k-exponent ($\eta = -2\alpha-2$) in S(k) spectra indicates the surface growth mechanism of the thin metal film.

2.8. Statistical analysis

The analyses of variance (ANOVA) were performed in GraphPad Prism 7 (Dotmatics, UK) software, using Tukey's test with a confidence level of 95%.

3. Results and discussion

3.1. Copper coating topography

The surface topography plays a critical role in the total surface free energy, microorganism attachment and biofilm formation on material surfaces [46]. Then, it is essential to evaluate surface parameters, such as surface roughness, to evaluate how the surface topography changed by the copper sputtering.

The AFM topographic images of the PLA films are shown in Fig. 2. The AFM images show that the copper coating leads to the formation of nanometric structures on the PLA surface, increasing its surface roughness. The height-height correlation function, H(r), and power spectral density function, S(k), were computed from the AFM data. The H(r) and S(k) curve profiles in Figs. 3a and 3b are typical characteristics of self-affine surfaces, which can be represented mathematically by rescaling a unitary geometry in horizontal and vertical directions as a fractal object [47].

These surfaces are characterized by a roughness exponent (α), also known as the static scaling exponent, and a growth exponent (β), also named the temporal scaling exponent. These exponents are adimensional parameters that universally specify the mechanism that guides the thin film growth and surface roughness evolution. The surface roughness of the thin film is a consequence of atomistic processes that co-occur [48]: (i) direct fixation of atoms on the surface of the substrate; (ii) remotion of surface atoms and atomic movements along the surface of the substrate and thin film during its formation; (iii) diffusive mass transport due to the formation of a potential chemical gradient in the surface during the thin film growing.

In self-affine surfaces, the root-mean-square (RMS) fluctuations of

Table 2
Static scaling exponent (roughness exponent, α), PSD k-exponent (η), and root-mean-square (RMS) roughness (also known as interface width, τ_{rms}) from height-height correlation function data for the PLA samples after different metal deposition times (0, 5, 10, and 20 s).

Copper deposition time (s)	Static scaling exponent / roughness exponent (α)	Root-mean-square (RMS) surface roughness / interface width - τ_{rms} (nm)	PSD k-exponent (η)
0	0.42 ± 0.02	1.06 ± 0.05	1.54 ± 0.15
5	0.64 ± 0.03	1.54 ± 0.08	2.49 ± 0.25
10	0.79 ± 0.04	1.93 ± 0.09	3.26 ± 0.33
20	0.66 ± 0.03	1.67 ± 0.08	2.78 ± 0.28

the surface height (τ_{rms}) present a dynamic scaling that follows a Family-Vicsek relationship (Eq. 5) [48].

$$\tau_{rms}(r,t) = t^{\beta} f\left(\frac{r}{t^{\beta/\alpha}}\right) \quad (5)$$

where $f\left(\frac{r}{t^{\beta/\alpha}}\right)$ is a constant, α and β are the roughness and growth exponents, respectively. Then, The temporal scaling exponent (growth exponent, β) calculated by fitting the root-mean-square (RMS) roughness (τ_{rms}) versus deposition time in a log-log plot (Fig. 3c) is 0.059 ± 0.153. As shown in Fig. 3d, the inclination of the log-log plot of the lateral correlation length (ξ) versus deposition time gives the dynamic exponent ($z = \alpha/\beta$), and the z value obtained here is 11.76 ± 0.58.

Table 2 details the α values obtained for the PLA samples estimated from the H(r) function. The copper deposition increases α. Also, the copper coatings present RMS surface roughness (interface width, τ_{rms}) slightly higher than that measured for the uncoated PLA. However, the copper coatings obtained by magnetron sputtering are smooth, with RMS surface roughness varying from 1 to 2 nm. The exponent of the power law region in the power spectral density (PSD) function, i.e., PSD k-exponent (η), indicates the surface growth mechanism of the copper coating is predominantly by bulk diffusion ($\eta = 3$), but evaporation-recondensation ($\eta = 2$) and surface diffusion ($\eta = 4$) may simultaneously occur too [49]. The surface roughness of the uncoated PLA is generated by a plastic flow ($\eta \sim 1$) with simultaneous evaporation-recondensation processes, which is coherent with the processing method used to prepare the PLA sample (i.e., casting of a viscous polymer solution).

The bulk diffusion involves the adsorption of copper atoms on the surface of the PLA substrate due to the high kinetical energy of these species after they eject the copper target. The copper atom ejection process is inherent from transfers of the kinetic moment caused by the bombing of the copper target with the argon atoms accelerated inside the vacuum chamber of the sputtering equipment [50]. Antagonistically, surface diffusion occurs through the lateral flow of these chemicals adsorbed on the PLA substrate surface from the deposition point to

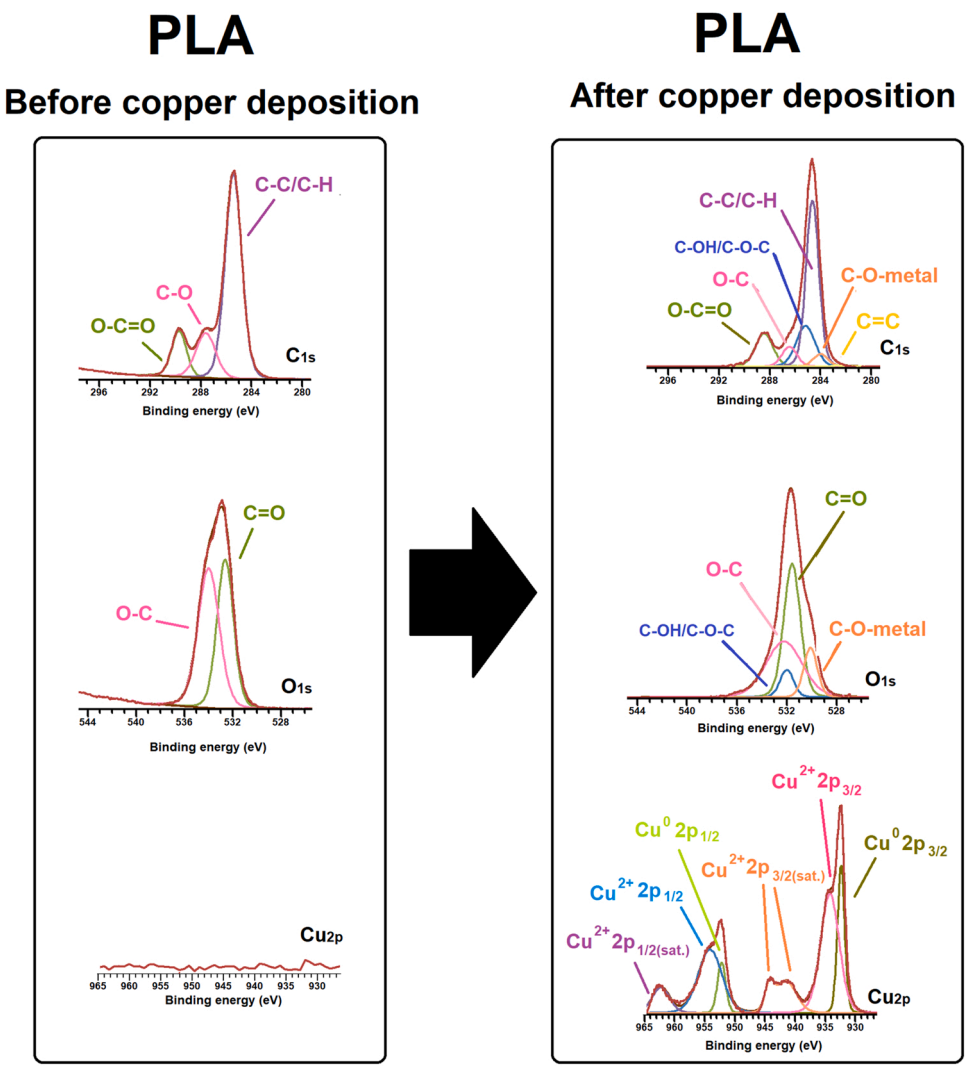

Fig. 4. $O_{1\,s}$, $C_{1\,s}$, and Cu_{2p} XPS high-resolution spectra regions from the PLA before and after copper deposition.

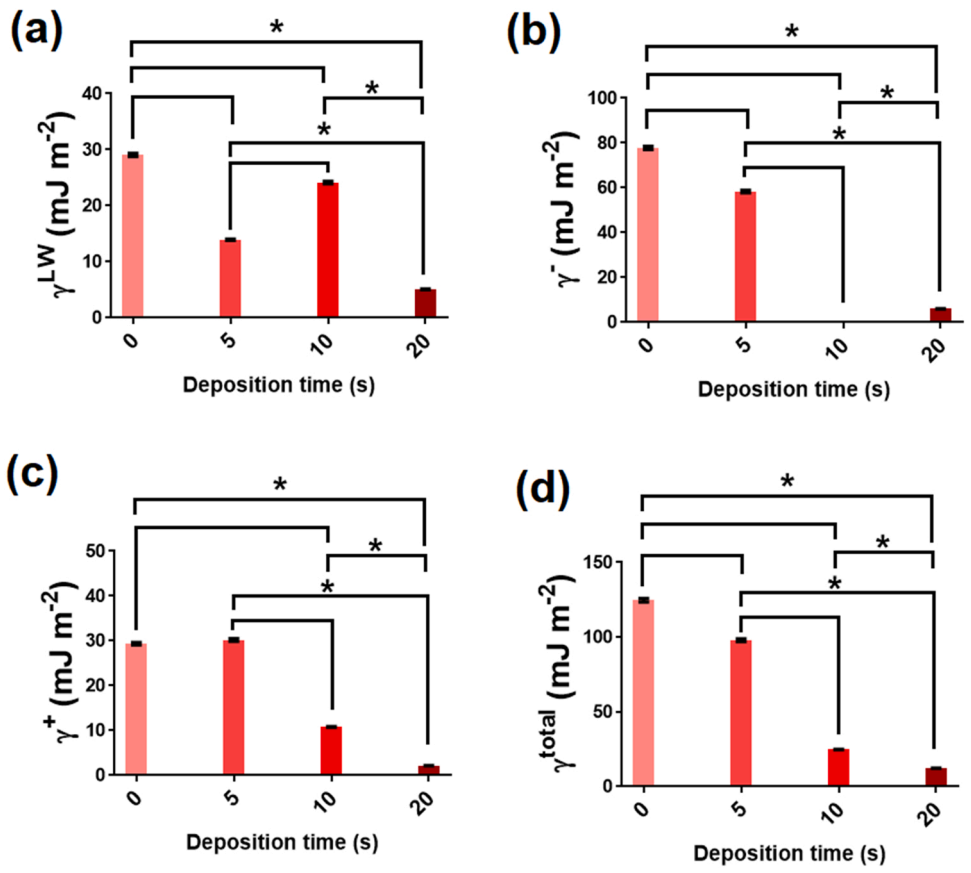

Fig. 5. (a) γ_s^{LW}, (b) γ_s^-, (c) γ_s^+, and (d) γ_s^{total} from the Cu-coated PLA films after different metal deposition times (0, 5, 10, and 20 s). The values are presented as mean ± standard deviation.*Values are significantly different according to Tukey's test and a 95% confidence level.

adjacent points onto the substrate surface, as illustrated in Fig. 3e.

3.2. Surface chemical structure and surface free energy

PLA presents characteristic electron binding energies in the $O_{1\,s}$ and $C_{1\,s}$ XPS high-resolution spectra regions at 287.1 eV (O-C, $C_{1\,s}$ region), 534.2 eV (O-C, $O_{1\,s}$ region), 289.7 eV (C═O, $C_{1\,s}$ region), 532.1 eV (C═O, $O_{1\,s}$ region), and 285.2 eV (C-C/C-H, $C_{1\,s}$ region) chemical bonds [51–54], as shown in Fig. 4. The copper deposition on the surface of this polymer leads to the formation of C═C (282.5 eV in $C_{1\,s}$ region), C-OH/C-O-C (285.1 eV in $C_{1\,s}$ region, 531.8 eV in $O_{1\,s}$ region), and C-O-Cu (283.8 eV in $C_{1\,s}$ region, 529.8 eV in $O_{1\,s}$ region) chemical bonds [55]. The C-OH, C═C, and C-O-C chemical linkages are inherently connected with the surface local degradation of the PLA polymer chains by random chain scissions. The sp^2 carbon (C═C) at 282,5 eV is not from carbides, according to the Cu_{2p} XPS region (Fig. 4). The sp^2 carbon (C═C) signal was shifted to electron binding energies slightly less than the data reported in the literature (284 – 285 eV) after the fitting process of the $C_{1\,s}$ spectrum due to overlapping with the C-C/C-H and C-O-Cu signals [56]. Also, the C-O-Cu signal was shifted to less electron binding energies than those reported in the literature, but surface effects must affect surface dipole moment that can cause shifting of the binding energies too [55,57].

The Cu_{2p} XPS spectral region also evidences the formation of copper metallic (Cu^0) on the copper coating: 932 (Cu^0 $2p_{3/2}$), 951.5 (Cu^0 $2p_{1/2}$) [58–61]. However, the XPS spectra in Fig. 4 also indicate Cu^{2+} on the Cu-coated PLA surface because there are XPS signals at 935 eV (Cu^{2+} $2p_{3/2}$) and 954.5 eV (Cu^{2+} $2p_{1/2}$) with XPS shake-up satellite signals with electron binding signals at 963.4 eV (Cu^{2+} $2p_{1/2}$ satellites), 944.2 eV (Cu^{2+} $2p_{3/2}$ satellites) and 941.2 eV (Cu^{2+} $2p_{3/2}$ satellites). The presence of Cu^{2+} can be associated with the C-O-Cu bonds that chemically link the copper coating to the PLA surface [58–61]. Also, Cu^{2+} can be from copper oxides that can be generated on the PLA surface due to oxidation of the copper coating with oxygen gas in the atmosphere, which is highly reactive immediately after removing Cu-coated PLA from the high vacuum sputtering chamber.

Hydrophobicity diminishes the adhesive interaction of microorganisms on the material surface, avoiding the attachment and proliferation of bacteria on surfaces contributing to the antimicrobial properties of materials. Besides antibacterial properties, hydrophobic surfaces are highly water-repellent and present other relevant technological and functional applications in aerospace, automotive, and biomedicine due to their anti-icing, self-cleaning, anti-fogging and other properties [62]. Then it is relevant to evaluate the alteration of surface free energy on PLA due to the chemical and morphological changes caused by the copper coating by sputtering.

The dispersive (γ_s^{LW}), acid (γ_s^+), and base (γ_s^-) components of the γ_s^{total} from contact angle measurements are shown in Fig. 5. These surface parameters were calculated with the generalized Wenzel-Cassie-Baxter, in which the surface roughness and other topographical parameters are considered to determine the surface free energy. For this purpose, the surface topographical parameters (not shown here) were determined from the AFM surface data of the PLA samples. The copper coating decreases γ_s^{LW}, γ_s^+, γ_s^- and γ_s^{total} of the PLA surface. Although there is the formation of carboxylic (COOH) and hydroxyl (OH) groups on the surface of the PLA films due to polymer degradation that could contribute to increasing the base (γ_s^-) components, the increase of copper metal content at the PLA surface attenuates the contribution of the chemical groups of the polymer at the surface to the polar (γ_s^p) component to the total surface free energy (γ_s^{total}) of the samples. The copper atomic

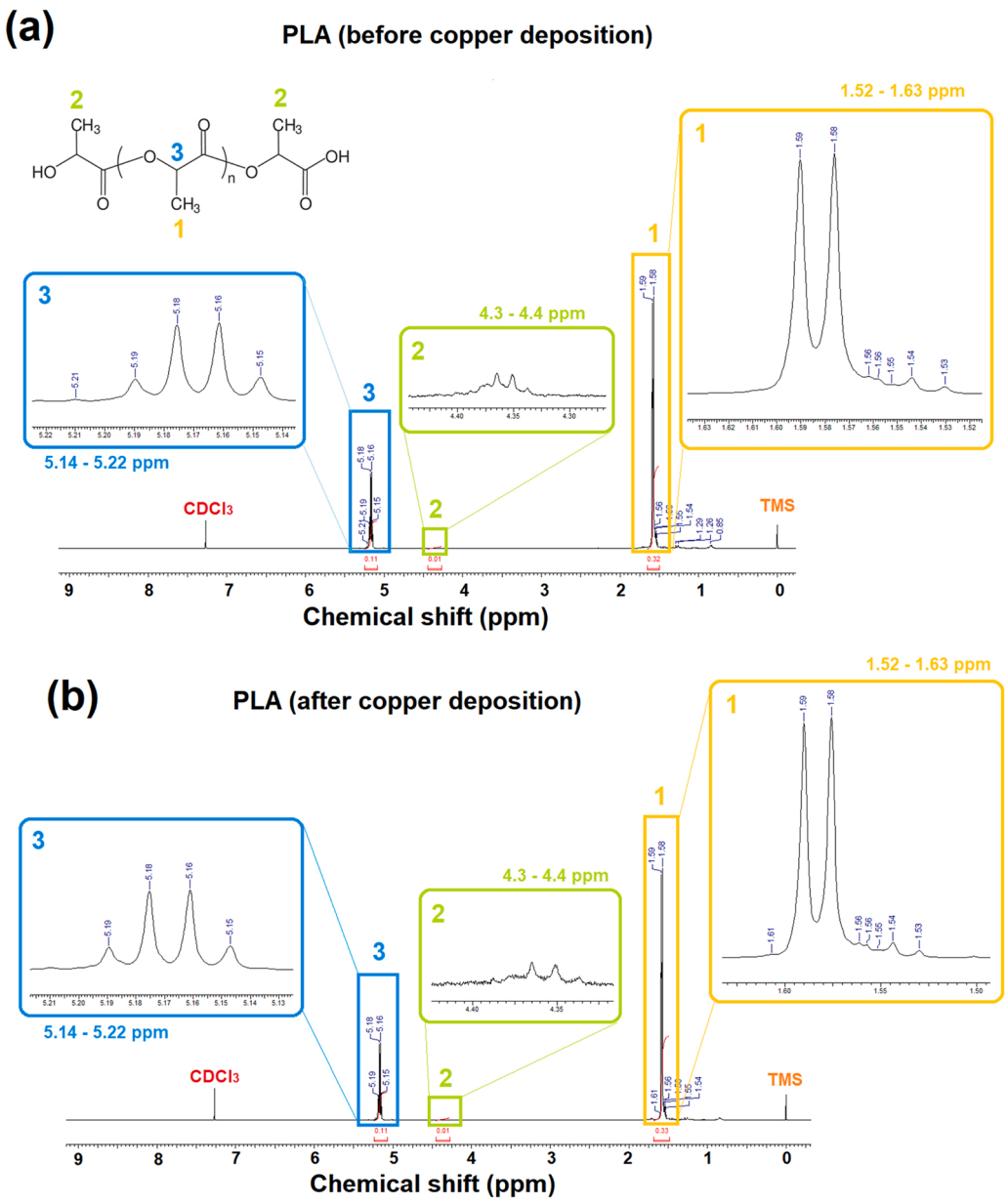

Fig. 6. ^{1}H NMR spectra of the PLA (a) before and (b) after copper deposition, using magnetron sputtering (copper deposition time = 20 s).

content on the PLA surface increases with increasing copper deposition time, while the total surface energy decreases with increasing copper sputtering time. The γ_s^{total} from the uncoated PLA sample is 124.67 ± 1.25 mJ.m^{-2}, being decreased to 97.89 ± 0.99 mJ.m^{-2} after 5 s of sputtering, 24.83 ± 0.25 mJ.m^{-2} after 10 s of sputtering, and 12.34 ± 0.12 mJ.m^{-2} after 20 s of sputtering. The γ_s^{total} value from uncoated PLA here is higher than 40–110 mJ.m^{-2} reported in the literature [63, 64], which must be associated with the fact that the γ_s^{total} values reported in the literature are calculated without considering the surface topographic parameters, disregarding surface defects and roughness, including the mathematical model and the measurement assay.

3.3. PLA bulk chemical structure

Typically, PLA suffers random chain scissions under plasma treatments, leading to degradation reactions. Also, oxidation processes may occur when water and oxygen gas are dissolved in the polymer bulk. However, the ^{1}H NMR spectra (Fig. 6) do not indicate the increase of subproducts with hydroxyl (2–4 ppm), anhydride (2–3 ppm) and vinyl (4.6–5.9 ppm), and carboxylic acid (2–2.6 ppm) moieties due to the reactions of free radicals carboxylic acid in PLA with the water and O_2 molecules [65]. Although the XPS spectroscopy indicated PLA degradation by polymer chain scission at the surface, there are no appreciable molecules with -COO–C- (esters, 3.7–4.1 and 2–2.6 ppm) and C═C (4.6–5.9 ppm) chemical bonds detected by NMR due to the PLA bulk degradation mechanisms via Norrish type I and type II, respectively [66–68]. Furthermore, the ^{1}H spectra indicate that the macroradicals generated on the surface of the PLA films during the process of copper deposition by magnetron sputtering do not have sufficient mobility to enter the PLA bulk and initiate degradation reactions within the film. These macroradicals are likely to be highly reactive, reacting immediately with neighboring chemical species on the PLA surface shortly after being formed during copper sputtering.

The ^{1}H NMR spectrum from uncoated PLA (Fig. 6a) exhibits the quadruple signal from =CH– asymmetric methine groups at 5.15, 5.16, 5.18, and 5.19 ppm. These quadruplet signals indicate the presence of

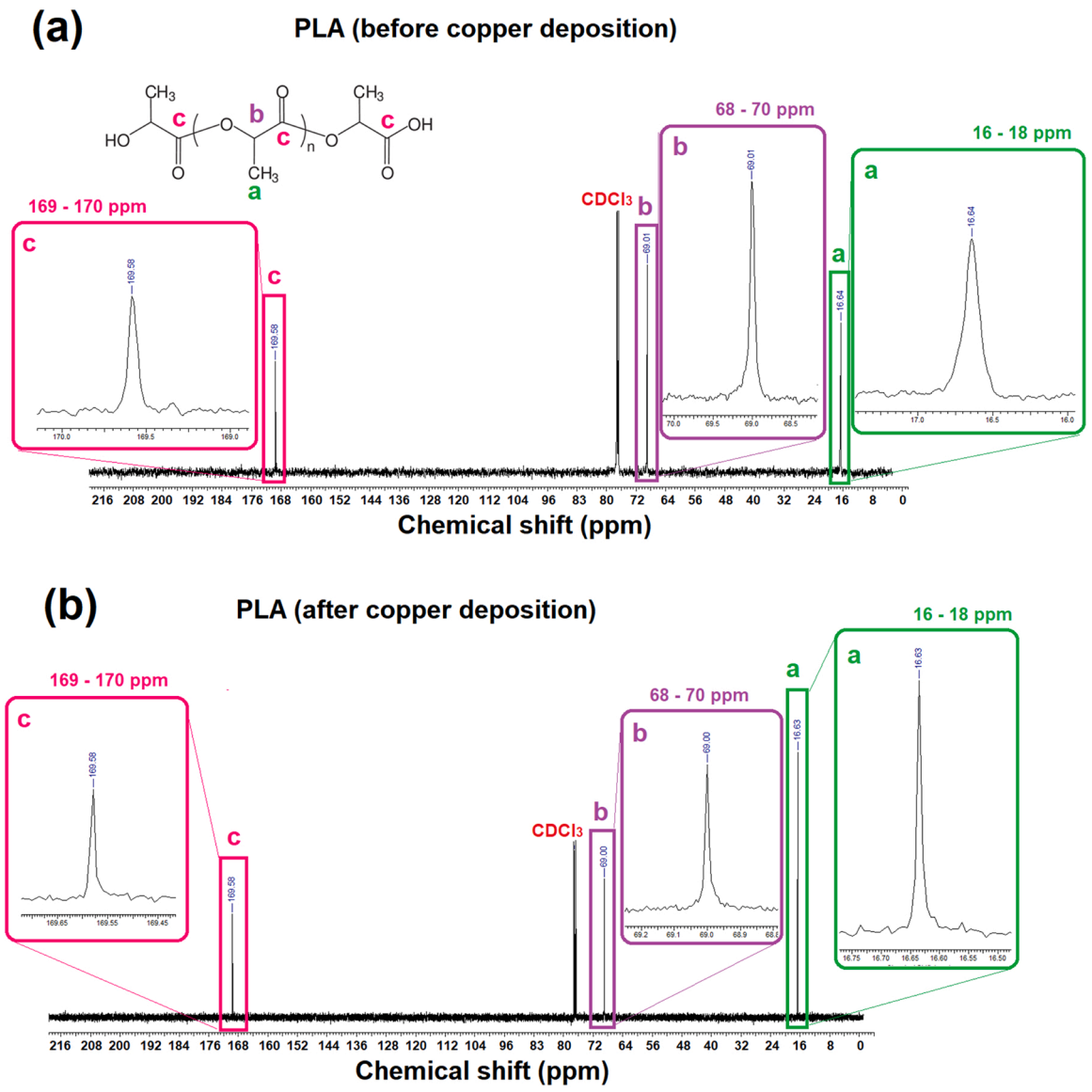

Fig. 7. ^{13}C NMR spectra of the PLA (a) before and (b) after copper deposition, using magnetron sputtering (copper deposition time = 20 s).

unique left- or right-handed (L or D) enantiomers along the PLA polymer chains (i.e., PLA isotactic) due to the coupling between CH and CH_3 protons in the PLA polymer backbone [69–71]. Moreover, there is a characteristic doublet signal from CH_3 protons (a doublet signal) with chemical shifts at 1.58 and 1.59 ppm. The multiple signals with low intensity and located at 4.35, 4.36, 4.37, and 4.38 ppm are attributed to protons from the terminal CH_3 groups linked to COOH end groups on the PLA polymer chains [72].

The degree of polymerization (i.e., the number of repeating units in the polymer, n) and the number-average molar weight (M_n) of the PLA are 11 and 881 g.mol^{-1}, respectively. n and M_n were estimated by the integration of the proton signal from the end-group (4.33 ppm) and the proton signal from the methine polymer repeating unit (5.18 ppm), according to Eqs. (6) and (7) [70]. Moreover, n and M_n do not suffer changes due to the copper deposition via magnetron sputtering, as shown in Fig. 6b.

$$n = \frac{\delta_{5.18\text{ppm}}}{\delta_{4.33\text{ppm}}} \tag{6}$$

$$M_n = 72n + 89 \tag{7}$$

The ^{13}C NMR spectra from the PLA sample (Fig. 7) present the characteristic carbon signal from C═O (170 ppm), CH_3 (16.6 ppm), and =CH– (69 ppm) chemical groups. The unique carbon signal at 69 ppm also suggests the PLA isotactic. The ^{1}H-^{13}C HSQC NMR spectra of the PLA before and after copper deposition (Figs. 8a and 8b) evidence confirm the correlations between the carbons and their attached protons along the PLA polymer backbone, except for the terminal CH_3 polymer chain groups due to their low amount in the PLA bulk. The ^{13}C NMR and ^{1}H-^{13}C HSQC NMR spectra of the PLA samples also confirm that there is no significant presence of PLA degradation by-products inside the PLA bulk due to the copper coating procedure. This characteristic PLA stability guarantees that this polymer does not change its macroscopic properties due to its surface coating with copper. The copper coating aims to confer only the antimicrobial properties to PLA without changes in other polymeric material properties that can be essential to its technological applications and durability since the macroradicals can trigger degradation reactions within the PLA bulk [65].

3.4. Antimicrobial assays

The antimicrobial and antibiofilm performances against *E. coli*

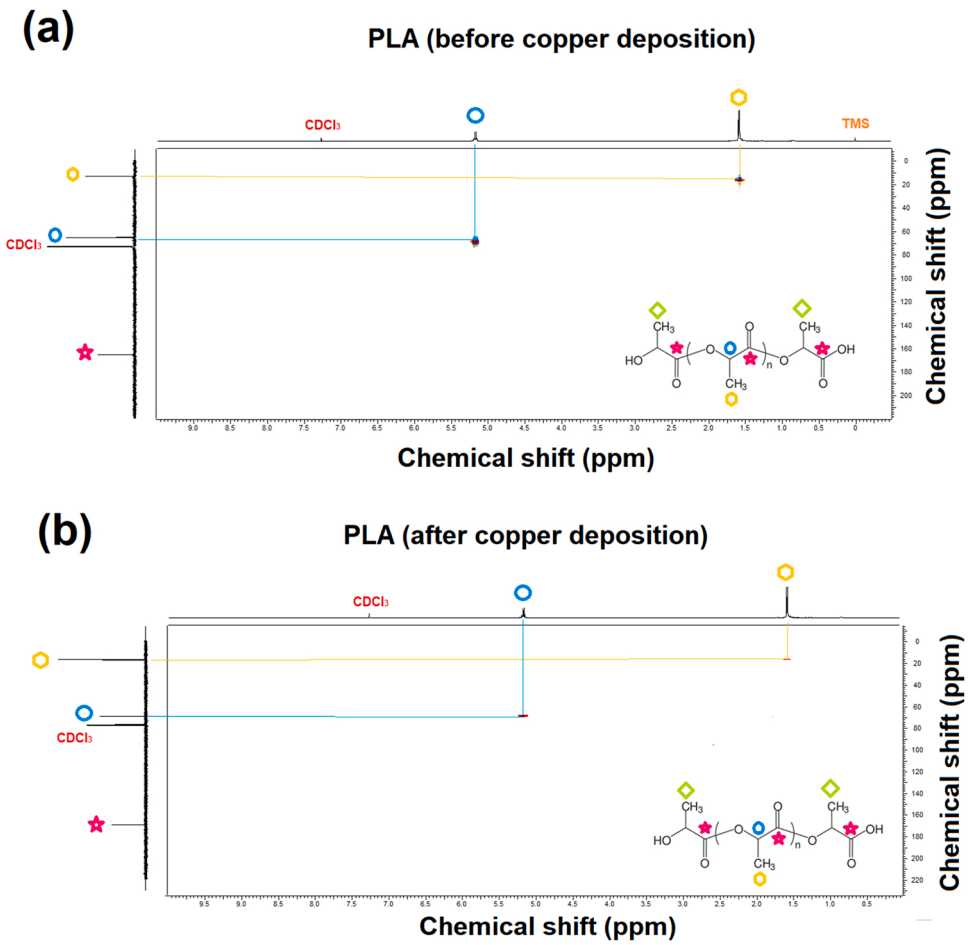

Fig. 8. ^{1}H-^{13}C HSQC NMR spectra of the PLA (a) before and (b) after copper deposition, using magnetron sputtering (copper deposition time = 20 s).

(Gram-negative bacteria, G-) and *S. subtilis* (Gram-positive bacteria, G+) of the Cu-coated PLA were evaluated via bacteria counting. PLA is known as a polymer that has no intrinsic antimicrobial activity. According to Figs. 9a and 9b, the antimicrobial tests show that only all copper-coated PLA samples show bactericidal activity, which corresponds to a bacterial reduction greater than 99.9% (i.e., ≥ 3 $\log_{10}$) of the total count of CFU.mL^{-1} concerning the uncoated PLA sample. These outstanding antimicrobial results from Cu-coated PLA samples evidence that the copper coating does not only inhibit the bacterial growth and reproduction of *E. coli* and *S. subtilis* strains (i.e., bacteriostatic activity with bacterial reduction of 99% (10^2 CFU.mL^{-1}, or 2 $\log_{10}$ CFU.mL^{-1}), but provoking the death of all those G- and G+ bacteria strains in direct contact with the metal coating on PLA surface. Bactericidal activity is of great interest to the hospital area to ensure the death or irreversibly damage of bacteria that are adhered to surfaces. The intrinsic antimicrobial properties of copper (metal and oxides) are from the oxidative mechanisms via metal ion releasing and generation of reactive oxygen species (ROS) that damage the bacteria cell constituents (proteins, lipids, DNA, and RNA) [73].

Non-thermal plasma technologies are attractive pathways for the surface modification of polymers from an ecological point of view because they cause less environmental impact since they involve a generation of low waste amounts [74–76]. The proper choice of plasma technology and the type of antimicrobial agent can be an effective way to give antimicrobial properties to polymers. Despite these benefits, there is a lack of work involving the copper metallic coating of PLA using such plasma technologies. Woskowicz et al. [77] used magnetron sputtering physical vapor deposition (MS-PVD) to coat polypropylene (PP) with silver and copper. The copper coatings led to a 100% reduction in cell viability of G+ (*Staphylococcus aureus*) and G- (*E. coli*) bacteria, but the coating process proposed by them is protracted (> 1 h) [77]. In addition to antimicrobial functions, copper coatings may be suitable for other applications. In the work of Arash and collaborators [78], copper coatings were used to enhance the durability of 3d printed structures of poly(acrylonitrile-butadiene-styrene) (ABS) against aggressive environmental conditions. Graphene has been considered a 2D tunable polymer [79], and copper nanoparticle coatings have been deposited in graphene by magnetron sputtering to make biosensors [80].

The antiviral performance of the Cu-coated PLA samples was investigated by the amplification of the Omicron SARS-CoV-2 genetic material by RT-qPCR (Fig. 9c), using the N2 nucleocapsid gene as a genetic target in the RT-qPCR experiments. The Omicron strain is a SARS-CoV-2 infectious variant able to escape the host immune mechanism response due to several mutations in RNA segments that are directly connected with the synthesis of structural and non-structural proteins that mediate and participate in the process of host infection by this virus [35]. Uncoated PLA does not have intrinsic antimicrobial activity [34], and the RNA amplified copies by RT-qPCR for this sample reached 5.18×10^5 copies.μL^{-1} after 30 min of direct contact with the viral inoculum. The decrease of RNA amplified copies of the uncoated PLA concerning the positive control is due to the viral structure compromising along exposition time in a harmful environment to the virions, since PLA does not present any intrinsic chemical or physical mechanisms to damage the RNA in the Omicron SARS-CoV-2 particles. Then, it is reasonable to assume that the antiviral assay causes irreversible damage to some SARS-CoV-2 virions, reducing the amount of RNA viral that posteriorly is amplified by RT-qPCR. The copper coating reduces the number of RNA amplified copies to values less than 1.2×10^6 copies.μL^{-1}, corresponding

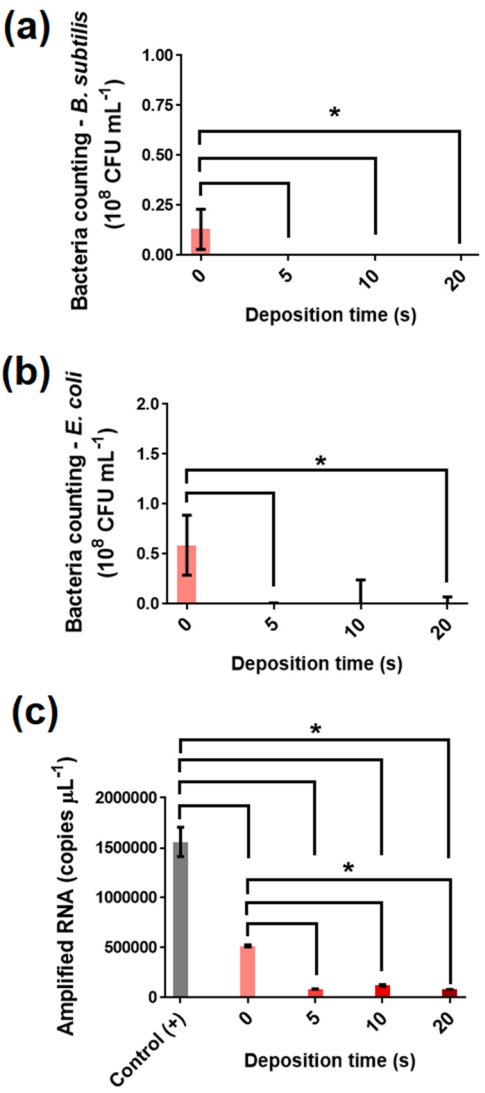

Fig. 9. (a) *B. subtilis* bacteria counting, (b) *E. coli* bacteria counting, and (c) amplified RNA by RT-qPCR for Omicron SARS-CoV-2 using the N2 gene targets of the Cu-coated PLA films after different metal deposition times (0, 5, 10, and 20 s). The values are presented as mean ± standard deviation.*Values are significantly different, according to Tukey's test and a 95% confidence level. Cycle threshold (Ct) values from RT-qPCR were lower than 30. Negative controls from the bacteria counting assays were $< 0.001 \times 10^8$ CFU mL^{-1}.

to a percentual reduction of 25–27% fold for the viral genetic material in Omicron SARS-CoV-2 inoculum after 30 min of direct contact with the uncoated PLA sample.

4. Conclusions

Antimicrobial copper coating on PLA surfaces was successfully obtained by magnetrons sputtering. The coating procedure leads to chemical and topographical changes in the PLA films. The copper coating reduces the total surface free energy of the PLA, making the PLA surface more hydrophobic leading to the formation of polymer degradation sub-products localized at the PLA surface via random polymer chain scission, while the polymer bulk was not compromised by the highly reactive conditions of magnetron sputtering that could trigger a runaway polymer degradation process by scission reactions of polymer chains in the PLA bulk. According to the AFM data and power spectral density (PSD) function, bulk diffusion is the primary growth mechanism of the copper coating on the PLA surface.

The Cu-coated PLA samples present bactericidal activity against *E. coli* and *S. subtilis*, hampering the formation and growth of bacterial biofilm onto the PLA surface. Moreover, the copper coating can reduce the genetic material of Omicron SARS-CoV-2 after 30 min of direct contact with an inoculum infected with viable viral particles. The results indicate a great potential for using copper coating via magnetron sputtering for the surface modification of PLA for multifunctional applications that require antimicrobial properties.

Declaration of Competing Interest

The authors declare that they have no known competing financial interests or personal relationships that could have appeared to influence the work reported in this paper.

Data Availability

Data will be made available on request.

Acknowledgments

The authors thank the CAPES (Code 001), UFABC no 48/2020 - REIT (11.01), REVALORES, UFABC, Nuclear and Energy Research Institute (IPEN-CNEN/SP), University of São Paulo (USP), Faculty of Medicine of ABC (FMABC), and Multiuser Central Facilities (UFABC) for the experimental support. We are grateful to Dr. André P. Tschiptschin, Dr. Newton K. Fukumasu, and Dr. Inés Pereyra for the experimental support with the plasma experiments in the Labplasma and Microelectronics laboratories at Polytechnic School, the University of São Paulo. This research used facilities of the Brazilian Nanotechnology National Laboratory (LNNano), part of the Brazilian Centre for Research in Energy and Materials (CNPEM), a private non-profit organization under the supervision of the Brazilian Ministry for Science, Technology, and Innovations (MCTI). We are grateful to the XPS and AFM staff of the LNNano for their assistance during the experiments (AFM-28009, XPS-20220130, and XPS-20220131 proposals).

Ethical Statement

This work was approved by the Local Ethical Committee of the Faculty of Medicine of ABC (FMABC) (4.427.013, 2020).

Funding

This research was funded by CAPES-Pandemias (88881.504639/2020–01), the Brazilian National Council of Scientific and Technological Development (305819/2017–8), and the Brazilian National Council of Scientific and Technological Development (CNPq) in partnership with Ministry of Science, Technology, Innovations and Communications (MCTIC), and Ministry of Health (MS), Secretariat of Science, Technology, Innovation and Strategic Inputs – Decit/SCTIE 07/2020 (Research to cope with COVID-19, its consequences and other severe acute respiratory syndromes – No. 402432/2020–7).

CRediT authorship contribution statement

Daniel José da Silva: Conceptualization, Methodology, Validation, Formal analysis, Investigation, Writing – original draft, Writing – review & editing, Visualization. **Greiciele S. Ferreira**: Conceptualization, Methodology, Validation. **Adriana Duran:** Conceptualization, Methodology, Validation, Formal analysis. **Fernando L. A. Fonseca**: Project administration, Resources, Funding acquisition. **Duclerc F. Parra:** Resources, Methodology, Formal analysis, Review. **Rodrigo F. Bueno**: Resources, Writing – review & editing, Supervision, Project administration, Funding acquisition. **Derval S. Rosa**: Resources, Writing – review & editing, Supervision, Project administration, Funding

acquisition.

References

[1] V. Kochkodan, N. Hilal, A comprehensive review on surface modified polymer membranes for biofouling mitigation, Desalination 356 (2015) 187–207, https://doi.org/10.1016/j.desal.2014.09.015.

[2] L. Cheng, M.D. Weir, H.H.K. Xu, J.M. Antonucci, A.M. Kraigsley, N.J. Lin, S. Lin-Gibson, X. Zhou, Antibacterial amorphous calcium phosphate nanocomposites with a quaternary ammonium dimethacrylate and silver nanoparticles, Dent. Mater. 28 (2012) 561–572, https://doi.org/10.1016/j.dental.2012.01.005.

[3] J.M. Antonucci, D.N. Zeiger, K. Tang, S. Lin-Gibson, B.O. Fowler, N.J. Lin, Synthesis and characterization of dimethacrylates containing quaternary ammonium functionalities for dental applications, Dent. Mater. 28 (2012) 219–228, https://doi.org/10.1016/j.dental.2011.10.004.

[4] P. Ferreira, P. Alves, P. Coimbra, M.H. Gil, Improving polymeric surfaces for biomedical applications: a review, J. Coat. Technol. Res 12 (2015) 463–475, https://doi.org/10.1007/s11998-015-9658-3.

[5] K. Madhavan Nampoothiri, N.R. Nair, R.P. John, An overview of the recent developments in polylactide (PLA) research, Bioresour. Technol. 101 (2010) 8493–8501, https://doi.org/10.1016/j.biortech.2010.05.092.

[6] M.L. Di Lorenzo, R. Androsch, Industrial Applications of Poly(lactic acid). Cham, Springer International Publishing, 2018, https://doi.org/10.1007/978-3-319-75459-8.

[7] R. Morent, N. De Geyter, T. Desmet, P. Dubruel, C. Leys, Plasma surface modification of biodegradable polymers: a review, Plasma Process. Polym. 8 (2011) 171–190, https://doi.org/10.1002/ppap.201000153.

[8] D.J. da Silva, H. Wiebeck, Current options for characterizing, sorting, and recycling polymeric waste, Prog. Rubber Plast. Recycl. Technol. 36 (2020) 284–303, https://doi.org/10.1177/1477760620918603.

[9] A. Elbourne, R.J. Crawford, E.P. Ivanova, Nano-structured antimicrobial surfaces: from nature to synthetic analogues, J. Colloid Interface Sci. 508 (2017) 603–616, https://doi.org/10.1016/j.jcis.2017.07.021.

[10] H. Gao, X. Fang, H. Chen, Y. Qin, F. Xu, T.Z. Jin, Physiochemical properties and food application of antimicrobial PLA film, Food Control 73 (2017) 1522–1531, https://doi.org/10.1016/j.foodcont.2016.11.017.

[11] R. Pantani, G. Gorrasi, G. Vigliotta, M. Murariu, P. Dubois, PLA-ZnO nanocomposite films: water vapor barrier properties and specific end-use characteristics, Eur. Polym. J. 49 (2013) 3471–3482, https://doi.org/10.1016/j.eurpolymj.2013.08.005.

[12] F. Valerio, M. Di Biase, V.M.T. Lattanzio, P. Lavermicocca, Improvement of the antifungal activity of lactic acid bacteria by addition to the growth medium of phenylpyruvic acid, a precursor of phenyllactic acid, Int. J. Food Microbiol. 222 (2016) 1–7, https://doi.org/10.1016/j.ijfoodmicro.2016.01.011.

[13] S. Milovanovic, G. Hollermann, C. Errenst, J. Pajnik, S. Frerich, S. Kroll, K. Rezwan, J. Ivanovic, Supercritical CO2 impregnation of PLA/PCL films with natural substances for bacterial growth control in food packaging, Food Res. Int. 107 (2018) 486–495, https://doi.org/10.1016/j.foodres.2018.02.065.

[14] W. Randazzo, M.J. Fabra, I. Falcó, A. López-Rubio, G. Sánchez, Polymers and biopolymers with antiviral activity: potential applications for improving food safety, Compr. Rev. Food Sci. Food Saf. 17 (2018) 754–768, https://doi.org/10.1111/1541-4337.12349.

[15] J.L. Castro-Mayorga, A. Martínez-Abad, M.F. Fabra, J.M. Lagarón, M.J. Ocio, G. Sánchez, Silver-based antibacterial and virucide biopolymers, in: Antimicrob Food Packag, Elsevier, 2016, pp. 407–416, https://doi.org/10.1016/B978-0-12-800723-5.00032-2.

[16] A. Martínez-Abad, M.J. Ocio, J.M. Lagarón, G. Sánchez, Evaluation of silver-infused polylactide films for inactivation of Salmonella and feline calicivirus in vitro and on fresh-cut vegetables, Int. J. Food Microbiol. 162 (2013) 89–94, https://doi.org/10.1016/j.ijfoodmicro.2012.12.024.

[17] D.C. Vodnar, L. Mitrea, L.F. Călinoiu, K. Szabo, B.E. Ştefănescu, Removal of bacteria, viruses, and other microbial entities by means of nanoparticles, in: Adv Nanostructures Environ Heal, Elsevier, 2020, pp. 465–491, https://doi.org/10.1016/B978-0-12-815882-1.00011-2.

[18] V. Lysenko, V. Lozovski, M. Lokshyn, Y.V. Gomeniuk, A. Dorovskih, N. Rusinchuk, Y. Pankivska, O. Povnitsa, S. Zagorodnya, V. Tertykh, Y. Bolbukh, Nanoparticles as antiviral agents against adenoviruses, Adv. Nat. Sci. Nanosci. Nanotechnol. 9 (2018), 025021, https://doi.org/10.1088/2043-6254/aac42a.

[19] F. Luzi, E. Fortunati, A. Jiménez, D. Puglia, A. Chiralt, L. Torre, P.L. A. Nanocomposites, Reinforced with cellulose nanocrystals from posidonia oceanica and ZnO nanoparticles for packaging application, J. Renew. Mater. 5 (2017) 103–115, https://doi.org/10.7569/JRM.2016.634135.

[20] G. Leite, M. Padoveze, Copper as an antimicrobial agent in healthcare: an integrative literature review, J. Infect. Control. 1 (2012) 33–36.

[21] I. Salah, I.P. Parkin, E. Allan, Copper as an antimicrobial agent: recent advances, RSC Adv. 11 (2021) 18179–18186, https://doi.org/10.1039/D1RA02149D.

[22] M.C. Sportelli, M. Izzi, E.A. Kukushkina, S.I. Hossain, R.A. Picca, N. Ditaranto, N. Cioffi, Can nanotechnology and materials science help the fight against SARS-CoV-2, Nanomaterials 10 (2020) 802, https://doi.org/10.3390/nano10040802.

[23] P. Merkl, S. Long, G.M. McInerney, G.A. Sotiriou, Antiviral activity of silver, copper oxide and zinc oxide nanoparticle coatings against sars-cov-2, Nanomaterials 11 (2021) 1312, https://doi.org/10.3390/nano11051312.

[24] K.S. Egorova, V.P. Ananikov, Toxicity of metal compounds: knowledge and myths, Organometallics 36 (2017) 4071–4090, https://doi.org/10.1021/acs.organomet.7b00605.

[25] Lo. Porto Palumbo, Favia, Plasma nano-texturing of polymers for wettability control: why, what and how, Coatings 9 (2019) 640, https://doi.org/10.3390/coatings9100640.

[26] C. Mezaroba, D. Becker, J. Nahorny, A.A.C. Recco, L.C. Fontana, Nano-rugosidade gerada em amostras de polímero PEAD através de plasma RF de N2/O2, Matér. (Rio Jan.) 23 (2018) 1–10, https://doi.org/10.1590/s1517-707620180004.0567.

[27] X.-Q. Tan, J.-Y. Liu, J.-R. Niu, J.-Y. Liu, J.-Y. Tian, Recent progress in magnetron sputtering technology used on fabrics, Mater. (Basel) 11 (2018) 1953, https://doi.org/10.3390/ma11101953.

[28] D. Lundin, T. Minea, J.T. Gudmundsson, High Power Impulse Magnetron Sputtering: Fundamentals, Technologies, Challenges and Applications, Elsevier,, Cambridge, UK, 2020, https://doi.org/10.1016/C2016-0-02463-4.

[29] P. Cools, N. De Geyter, R. Morent, PLA enhanced via plasma technology: a review, in: C. Winthrop (Ed.), New Dev. Polylactic Acid Res., Polymer Sc, Nova Science Publishers, New York, 2015, pp. 79–110.

[30] G. Chen, Y. Chen, N. Jin, J. Li, S. Dong, S. Li, Z. Zhang, Y. Chen, Zein films with porous polylactic acid coatings via cold plasma pre-treatment, Ind. Crops Prod. 150 (2020), 112382, https://doi.org/10.1016/j.indcrop.2020.112382.

[31] I.R. Durán, S. Vanslambrouck, P. Chevallier, C.A. Hoesli, G. Laroche, Atmospheric pressure cold plasma versus wet-chemical surface treatments for carboxyl functionalization of polylactic acid: a first step toward covalent immobilization of bioactive molecules, Colloids Surf. B Biointerfaces 189 (2020), 110847, https://doi.org/10.1016/j.colsurfb.2020.110847.

[32] C. Park, Y.-J. Seong, I.-G. Kang, E.-H. Song, H. Lee, J. Kim, H.-D. Jung, H.-E. Kim, T.-S. Jang, Enhanced osseointegration ability of Poly(lactic acid) via tantalum sputtering-based plasma immersion ion implantation, ACS Appl. Mater. Interfaces 11 (2019) 10492–10504, https://doi.org/10.1021/acsami.8b21363.

[33] F. Rezaei, A. Nikiforov, R. Morent, N. De Geyter, Plasma modification of poly lactic acid solutions to generate high quality electrospun PLA nanofibers, Sci. Rep. 8 (2018) 2241, https://doi.org/10.1038/s41598-018-20714-5.

[34] A. Popelka, A. Abdulkareem, A.A. Mahmoud, M.G. Nassr, M.A. Al-Ruweidi, K. J. Mohamoud, M.K. Hussein, M. Lehocky, D. Vesela, P. Humpolíček, P. Kasak, Antimicrobial modification of PLA scaffolds with ascorbic and fumaric acids via plasma treatment, Surf. Coat. Technol. 400 (2020), 126216, https://doi.org/10.1016/j.surfcoat.2020.126216.

[35] M. Shah, H.G. Woo, Omicron: a heavily mutated SARS-CoV-2 variant exhibits stronger binding to ACE2 and potently escapes approved COVID-19 therapeutic antibodies, Front. Immunol. 12 (2022) 1–10, https://doi.org/10.3389/fimmu.2021.830527.

[36] M. Baibarac, L. Stingescu, M. Stroe, C. Negrila, E. Matei, L.C. Cotet, I. Anghel, I. E. Şofran, L. Baia, Poly(Vinyl Chloride) spheres coated with graphene oxide sheets: from synthesis to optical properties and their applications as flame-retardant agents, Polym. (Basel) 13 (2021) 565, https://doi.org/10.3390/polym13040565.

[37] R. Ramachandran, M. Nosonovsky, Coupling of surface energy with electric potential makes superhydrophobic surfaces corrosion-resistant, Phys. Chem. Chem. Phys. 17 (2015) 24988–24997, https://doi.org/10.1039/c5cp04462f.

[38] M. Nosonovsky, B. Bhushan, Patterned nonadhesive surfaces: superhydrophobicity and wetting regime transitions, Langmuir 24 (2008) 1525–1533, https://doi.org/10.1021/la702239w.

[39] D.J. da Silva, D.S. Rosa, Antimicrobial performance of bioinspired PLA fabricated via one-step plasma etching with silver and copper, ACS Appl. Polym. Mater. 4 (2022) 7162–7172, https://doi.org/10.1021/acsapm.2c01043.

[40] G. Hwang, C.H. Lee, I.S. Ahn, B.J. Mhin, Determination of reliable Lewis acid-base surface tension components of a solid in LW-AB approach, J. Ind. Eng. Chem. 17 (2011) 125–129, https://doi.org/10.1016/j.jiec.2010.12.009.

[41] F. Wen, Y. Cao, Y. Zhou, On studying surface and nanomechanical properties of Ti-O films by alkali treatment, Appl. Mech. Mater. 138– 139 (2011) 821–825, https://doi.org/10.4028/www.scientific.net/AMM.138-139.821.

[42] C.M. Vicente, P.S. André, R.A.S. Ferreira, Simple measurement of surface free energy using a web cam, Rev. Bras. Ensino Física 34 (2012), https://doi.org/10.1590/S1806-11172012000300012.

[43] I. Jordanov, B. Mangovska, Characterization on surface of mercerized and enzymatic scoured cotton after different temperature of drying, Open Text. J. 2 (2009) 39–47, https://doi.org/10.2174/1876520300902010039.

[44] T. Kallio, J. Laine, P. Stenius, Intermolecular interactions and the adhesion of oleic acid, J. Dispers. Sci. Technol. 30 (2009) 222–230, https://doi.org/10.1080/01932690802500719.

[45] D.J. da Silva, A.G. Souza, G. da, S. Ferreira, A. Duran, A.D. Cabral, F.L.A. Fonseca, R.F. Bueno, D.S. Rosa, Cotton fabrics decorated with antimicrobial Ag-coated TiO2 nanoparticles are unable to fully and rapidly eradicate SARS-CoV-2, ACS Appl. Nano Mater. 4 (2021) 12949–12956, https://doi.org/10.1021/acsanm.1c03492.

[46] A. Jaggessar, H. Shahali, A. Mathew, P.K.D.V. Yarlagadda, Bio-mimicking nano and micro-structured surface fabrication for antibacterial properties in medical implants, J. Nanobiotechnol. 15 (2017) 64, https://doi.org/10.1186/s12951-017-0306-1.

[47] M. Pelliccione, T.-M. Lu, Evolution of Thin Film Morphology, Springer New York, New York, NY, 2008, https://doi.org/10.1007/978-0-387-75109-2.

[48] I. Gupta, B.C. Mohanty, Dynamics of surface evolution in semiconductor thin films grown from a chemical bath, Sci. Rep. 6 (2016) 33136, https://doi.org/10.1038/srep33136.

[49] W.M. Tong, R.S. Williams, Kinetics of surface growth: phenomenology, scaling, and mechanisms of smoothening and roughening, Annu. Rev. Phys. Chem. 45 (1994) 401–438, https://doi.org/10.1146/annurev.pc.45.100194.002153.

[50] N. Gopalakrishnan, E.R. Messmer, S. Lourdudoss, Self consistent model For InP selective regrowth by hydride vapour phase epitaxy, Jpn. J. Appl. Phys. 38 (1999) 1037–1039, https://doi.org/10.1143/JJAP.38.1037.

[51] A. Koterwa, I. Kaczmarzyk, S. Mania, M. Cieslik, R. Tylingo, T. Ossowski, R. Bogdanowicz, P. Niedziałkowski, J. Ryl, The role of electrolysis and enzymatic hydrolysis treatment in the enhancement of the electrochemical properties of 3D-printed carbon black/poly(lactic acid) structures, Appl. Surf. Sci. 574 (2022), 151587, https://doi.org/10.1016/j.apsusc.2021.151587.
[52] F. Renò, D. D'Angelo, G. Gottardi, M. Rizzi, D. Aragno, G. Piacenza, F. Cartasegna, M. Biasizzo, F. Trotta, M. Cannas, Atmospheric pressure plasma surface modification of poly(D,L-lactic acid) increases fibroblast, osteoblast and keratinocyte adhesion and proliferation, Plasma Process. Polym. 9 (2012) 491–502, https://doi.org/10.1002/ppap.201100139.
[53] O. Laput, I. Vasenina, M.C. Salvadori, K. Savkin, D. Zuza, I. Kurzina, Low-temperature plasma treatment of polylactic acid and PLA/HA composite material, J. Mater. Sci. 54 (2019) 11726–11738, https://doi.org/10.1007/s10853-019-03693-4.
[54] Y. Qi, H.-L. Ma, Z.-H. Du, B. Yang, J. Wu, R. Wang, X.-Q. Zhang, Hydrophilic and antibacterial modification of poly(lactic acid) films by γ-ray irradiation, ACS Omega 4 (2019) 21439–21445, https://doi.org/10.1021/acsomega.9b03132.
[55] A.B. Siddique, A.K. Pramanick, S. Chatterjee, M. Ray, Amorphous carbon dots and their remarkable ability to detect 2,4,6-trinitrophenol, Sci. Rep. 8 (2018) 1–10, https://doi.org/10.1038/s41598-018-28021-9.
[56] X. Chen, X. Wang, D. Fang, A review on C1s XPS-spectra for some kinds of carbon materials, Fuller., Nanotub. Carbon Nanostruct. 28 (2020) 1048–1058, https://doi.org/10.1080/1536383X.2020.1794851.
[57] G. Greczynski, L. Hultman, The same chemical state of carbon gives rise to two peaks in X-ray photoelectron spectroscopy, Sci. Rep. 11 (2021) 11195, https://doi.org/10.1038/s41598-021-90780-9.
[58] D.J. da Silva, R.F. da Silva Barbosa, A.G. de Souza, R.R. Ferreira, P.H. Camani, I. L. Nantes-Cardoso, D.S. Rosa, Bactericidal activity of cotton fabrics functionalized by ZnO and Cu via microwave, Cellulose 28 (2021) 8153–8175, https://doi.org/10.1007/s10570-021-03990-9.
[59] B. Rebhan, S. Tollabimazraehno, G. Hesser, V. Dragoi, Analytical methods used for low temperature Cu–Cu wafer bonding process evaluation, Microsyst. Technol. 21 (2015) 1003–1013, https://doi.org/10.1007/s00542-015-2446-2.
[60] N.T. Bui, H. Kang, S.J. Teat, G.M. Su, C.-W. Pao, Y.-S. Liu, E.W. Zaia, J. Guo, J.-L. Chen, K.R. Meihaus, C. Dun, T.M. Mattox, J.R. Long, P. Fiske, R. Kostecki, J. J. Urban, A nature-inspired hydrogen-bonded supramolecular complex for selective copper ion removal from water, Nat. Commun. 11 (2020) 3947, https://doi.org/10.1038/s41467-020-17757-6.
[61] B. Wang, C. Zhao, H. Lu, T. Zou, S.C. Singh, Z. Yu, C. Yao, X. Zheng, J. Xing, Y. Zou, C. Tong, W. Yu, B. Zhao, C. Guo, SERS study on the synergistic effects of electric field enhancement and charge transfer in an Ag 2 S quantum dots/plasmonic bowtie nanoantenna composite system, Photonics Res 8 (2020) 548, https://doi.org/10.1364/PRJ.383612.
[62] K. Manoharan, S. Bhattacharya, Superhydrophobic surfaces review: functional application, fabrication techniques and limitations, J. Micro 2 (2019) 59–78, https://doi.org/10.1177/2516598419836345.
[63] A. Antunes, A.S. Luyt, P. Kasak, O. Aljarod, M.K. Hassan, A. Popelka, Effect of plasma treatment on accelerated PLA degradation, Express Polym. Lett. 15 (2021) 725–743, https://doi.org/10.3144/expresspolymlett.2021.60.
[64] J. Žigon, M. Karlž, M. Pavlič, Surface finishing of 3d-printed polymers with selected coatings, Polym. (Basel) 12 (2020) 1–14, https://doi.org/10.3390/polym12122797.
[65] A. Chamas, H. Moon, J. Zheng, Y. Qiu, T. Tabassum, J.H. Jang, M. Abu-Omar, S. L. Scott, S. Suh, Degradation rates of plastics in the environment, ACS Sustain. Chem. Eng. 8 (2020) 3494–3511, https://doi.org/10.1021/acssuschemeng.9b06635.
[66] M. Niaounakis, Biopolymers: Applications and Trends, William Andrew, Oxford, 2015.
[67] M. Niaounakis, Biopolymers: Reuse, Recycling, and Disposal, William Andrew, Oxford, 2013.
[68] W. Sakai, N. Tsutsumi, Photodegradation and radiation degradation, in: R. Auras, L.-T. Lim, S.E.M. Selke, H. Tsuji (Eds.), Poly(Lactic Acid), John Wiley & Sons, Inc, Hoboken, NJ, USA, 2010, pp. 413–421, https://doi.org/10.1002/9780470649848.ch24.
[69] K. Suganuma, T. Asakura, M. Oshimura, T. Hirano, K. Ute, H.N. Cheng, NMR analysis of poly(lactic acid) via statistical models, Polym. (Basel) 11 (2019) 725, https://doi.org/10.3390/polym11040725.
[70] J.M. Pérez, C. Ruiz, I. Fernández, Synthesis of a biodegradable PLA: NMR signal deconvolution and end-group analysis, J. Chem. Educ. 99 (2022) 1000–1007, https://doi.org/10.1021/acs.jchemed.1c00824.
[71] E. Dellacasa, L. Zhao, G. Yang, L. Pastorino, G.B. Sukhorukov, Fabrication and characterization of novel multilayered structures by stereocomplexion of poly(D-lactic acid)/poly(L-lactic acid) and self-assembly of polyelectrolytes, Beilstein J. Nanotechnol. 7 (2016) 81–90, https://doi.org/10.3762/bjnano.7.10.
[72] C.A. Ramírez-Herrera, A.I. Flores-Vela, A.M. Torres-Huerta, M.A. Domínguez-Crespo, D. Palma-Ramírez, PLA degradation pathway obtained from direct polycondensation of 2-hydroxypropanoic acid using different chain extenders, J. Mater. Sci. 53 (2018) 10846–10871, https://doi.org/10.1007/s10853-018-2380-7.
[73] S.M. Imani, L. Ladouceur, T. Marshall, R. Maclachlan, L. Soleymani, T.F. Didar, Antimicrobial nanomaterials and coatings: current mechanisms and future perspectives to control the spread of viruses including SARS-CoV-2, ACS Nano 14 (2020) 12341–12369, https://doi.org/10.1021/acsnano.0c05937.
[74] G. Hazell, L.E. Fisher, W.A. Murray, A.H. Nobbs, B. Su, Bioinspired bactericidal surfaces with polymer nanocone arrays, J. Colloid Interface Sci. 528 (2018) 389–399, https://doi.org/10.1016/j.jcis.2018.05.096.
[75] Y. Liu, J. Genzer, M.D. Dickey, "2D or not 2D": shape-programming polymer sheets, Prog. Polym. Sci. 52 (2016) 79–106, https://doi.org/10.1016/j.progpolymsci.2015.09.001.
[76] S. Kim, U.T. Jung, S.-K. Kim, J.-H. Lee, H.S. Choi, C.-S. Kim, M.Y. Jeong, Nanostructured multifunctional surface with antireflective and antimicrobial characteristics, ACS Appl. Mater. Interfaces 7 (2015) 326–331, https://doi.org/10.1021/am506254r.
[77] E. Woskowicz, M. Lozynska, A. Kowalik-Klimczak, J. Kacprzynska-Golacka, E. Osuch-Slomka, A. Piasek, L. Gradon, Plasma deposition of antimicrobial coatings based on silver and copper on polypropylene, Polimery 65 (2020) 33–43, https://doi.org/10.14314/polimery.2020.1.5.
[78] A. Afshar, D. Mihut, Enhancing durability of 3D printed polymer structures by metallization, J. Mater. Sci. Technol. 53 (2020) 185–191, https://doi.org/10.1016/j.jmst.2020.01.072.
[79] V. Palermo, Not a molecule, not a polymer, not a substrate… the many faces of graphene as a chemical platform, Chem. Commun. 49 (2013) 2848, https://doi.org/10.1039/c3cc37474b.
[80] T. Soganci, R. Ayranci, E. Harputlu, K. Ocakoglu, M. Acet, M. Farle, C.G. Unlu, M. Ak, An effective non-enzymatic biosensor platform based on copper nanoparticles decorated by sputtering on CVD graphene, Sens. Actuators B Chem. 273 (2018) 1501–1507, https://doi.org/10.1016/j.snb.2018.07.064.